Supplementary text C: Calculations and modelling

This supplement details (C1) dyke and sheet thickness distributions and how these vary between three study areas, (C2) how modal phase proportions in Tables 1-3 were derived, and (C3) how bulk rock geochemical HMD and LMD trends were reversely modelled for a more primitive and more evolved fractionating/accumulating assemblage of three phases, resulting in the main paper's Figure 10(g-h).

C1. Dyke and sheet thickness distributions

Dyke and sheet thicknesses were recorded in the field by both geological surveyors and, within study areas S, C & N, by the first author, and compiled onto the map in Figure C1(a). Any significant variation at sample sites along the same dyke (outside the study areas) may indicate that more than 11 dykes were sampled by others, unless individual dykes are locally irregular, e.g., at magmatic offsets.

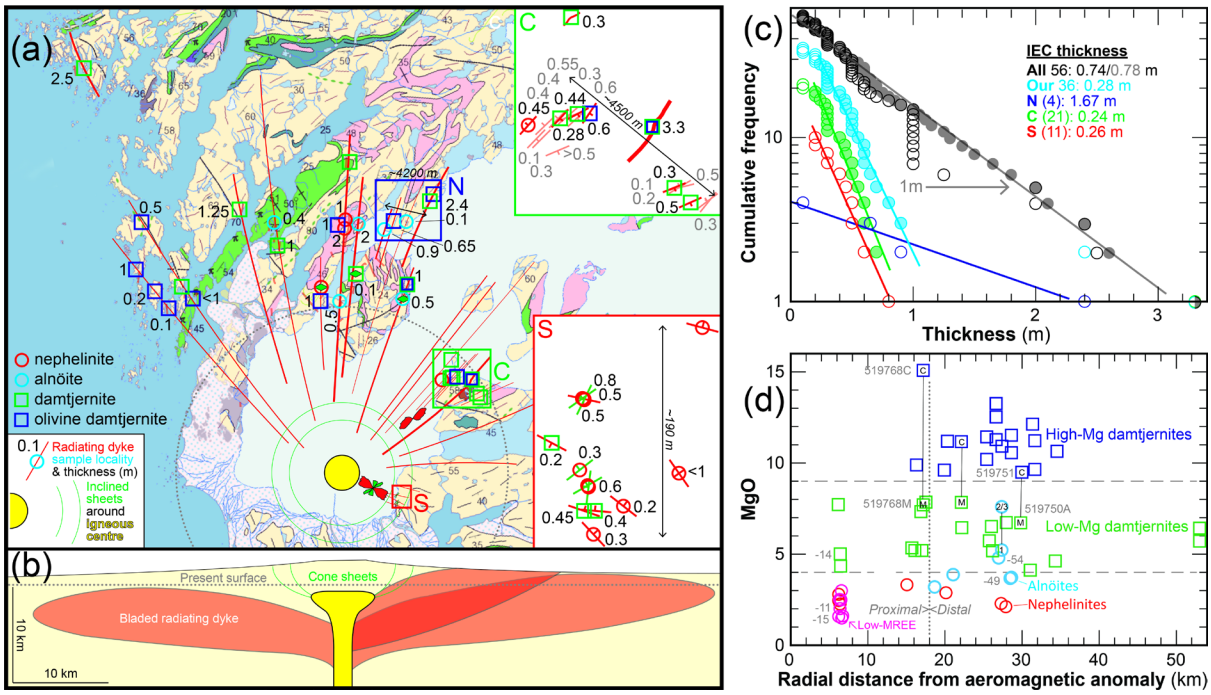

Figure C1: Dyke and sheet thicknesses. (a) Geological map, as in Figure 2(e), but showing recorded thicknesses in meters. Subdued grey numbers in study area C represent intrusions that were not sampled. (b) Schematic cross-section, as in Figure 2(h). (c) Dyke/sheet thickness distributions for various sample populations, as explained and discussed in the text. (d) Rock type distributions, as a function of how far from a common magmatic center these were sampled.

As expected for cogenetic dyke swarms, available 56 thickness measurements/estimates on FHI's lamprophyre dykes and sheets conform to a negative exponential distribution (Fig. C1c), expressed as straight lines in thickness versus logarithmic cumulative frequency diagrams (Jolly & Sanderson, 1995). However, one also notes a tendency for geological surveyors to round to a nearest whole or half meter (most obviously down to 1 m), where the swarm's real thickness distribution more likely conforms to adjusted data, shown by grey fills in Figure C1(c). These adjusted data have an arithmetic mean thickness of 0.76 m, or a more appropriate inverse exponential coefficient (IEC) of 0.78 m (for details see Klausen, 2006). A steeper negative exponential distribution is obtained, however, when only plotting the 36 dyke and sheet thicknesses from more proximally located study areas S, C and N (cyan data in Fig. C1c). Since the slope of this sub-population is steeper, it contains a greater number of thinner dykes, quantified by a more negative exponential coefficient, the inverse of which provides a narrower 'mean' IEC-thickness of 0.28 m. In other words, there is a greater number of thinner proximal intrusions, as expected since thinner intrusions freeze within a shorter distance from a source than thicker intrusions.

The effect of fewer dykes being able to propagate farther from their source will, combined with a radial spread from the igneous centre, invariably result in an exponential decline in the total amount of crustal dilation by dykes and sheets. This is quantified for each of the completely mapped study areas, where cumulative thicknesses of 4.3, 9.9 & 4.1 m by 14, 18 & 4 intrusions across ~950, ~4200 & ~4500 m-wide traverses (cf., Fig. 2e), result in 0.45, 0.24 & 0.09 % of magmatic dilation at study areas S, C and N, located ~6.5, ~16.5 & ~28 km from the aeromagnetic anomaly, respectively; reflecting an expected increased 'magmatism' towards a common central source. This, despite the thickness distribution for study area N only consisting of four dykes, dominated by a 2.4 m-thick dyke (Samples 519750-1).

Finally, Figure C1(d) shows how sampled rock types vary with distance from a common magmatic center, where most nephelinites (at least their low-MREE sub-group) were emplaced more proximally to the igneous center. All HMD samples were collected >16 km from the igneous center, consistent with thicker dykes (with porphyritic HMD cores) being able to propagate farther than thinner dykes and possibly as bladed dykes that propagated obliquely upwards from deeper magma chamber source regions (Fig. C1b). However, sampled alnöites are equally distant, while LMD samples were collected throughout. The sampling by others of different rock types apparently along the same dyke may in some cases not be a problem since individual dykes are known to have both aphyric LMD margins and porphyritic HMD cores. However, in two cases where LMD and alnöite samples, and in another case where a HMD and a nephelinite sample, were apparently collected from along the same dyke (cf., Fig. C1a), it seems more likely for several different dykes being present along the same mapped trend than individual dykes being as composite as that.

C2. Modal phase proportions

Modal phase proportions are based on both (1) traced thin sections (Figs. B1e-f, B2a-c & 7a), and (2) traced SEM elemental and electron backscatter maps (Figs. B5b, 4f-g, 5, 6b & 7b-d). Areal calculations were made in Adobe Illustrator, using a plug-in script freeware. While it is straight-forward to calculate proportions that way for different phenocryst types, ocelli and remaining matrixes (Tables B1 & 1), as well as all different phases inside selected ocelli and smaller matrix-areas (Tables 2-3), there were some challenges in extrapolating results to the rest of the thin section. For the more homogeneous matrixes of HMD-sample 519751 and alnöite sample 519745, it was simply a matter of expanding proportions to the rest of the thin section's area, subtracted by any phenocrysts and ocelli. For the more heterogenous nephelinite sample 519715, however, phase proportions were first determined for both the more carbonaceous patch and surrounding analcime-rich parts of the 6.6 mm^2-large SEM-mapped matrix area. Proportions within the carbonaceous patch could then be expanded into 5.7% of this thin section (cf., Fig. 7a), mapped as being made up of a similar greyish matrix type as the patch. Proportions within the analcime-rich part were expanded into the rest of the thin section, excluding the greyish matrix type as well as any pale veins and ocelli (2.3% of this thin section). Similar calculations were made for ratios between analcime and carbonates (last column in Table 3), where ocelli and veins naturally had a higher proportion of these very late stage phases.

From the phase proportions within four ocelli from HMD dyke core sample 519751, it was possible to calculate bulk concentrations in major oxides within each (e.g., yellow circles in Figs. 9 & C2-3), by multiplying individual phase proportions with a stoichiometric composition of each phase. These compositions were as close as possible to measured average solid-solution compositions, determined by SEM (Fig. B9).

C3. Reverse modelling of geochemical damtjernite trends

The applied 2D graphical reverse modelling of bulk rock geochemical trends can only be applied to a maximum of three phases, in this case likely earliest crystallizing olivine, augite and magnetite, as

well as substituting olivine for later crystallizing biotite. The modelling further uses SEM spot analysed compositions on phenocrysts (Fig. B9), together with four ocelli (yellow) that – as mentioned – were calculated from their phase proportions in Figure 5 and their stoichiometric formulae, adjusted to measured average solid solution compositions.

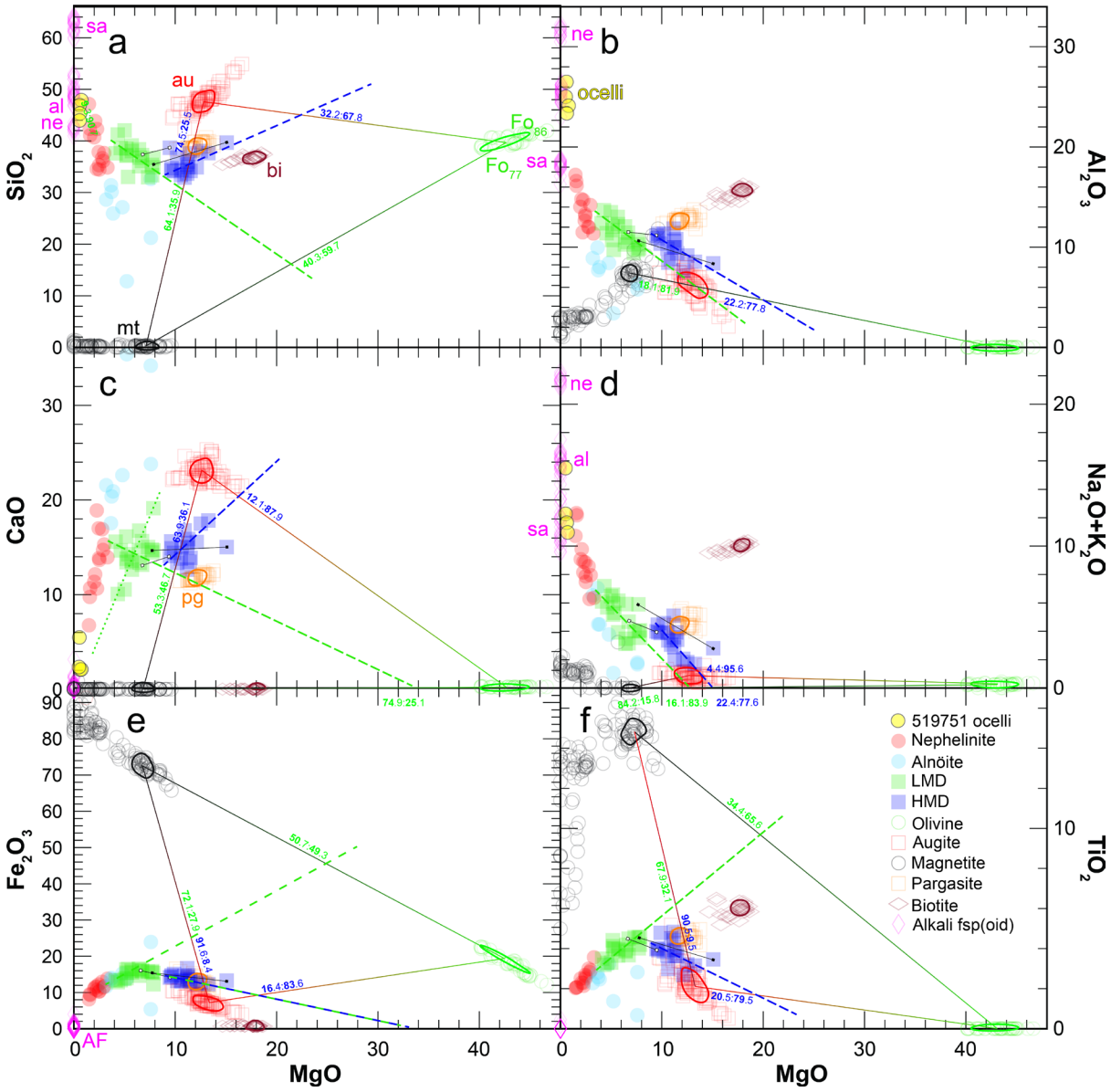

Figure C2: Enlarged versions of previous major element variation diagrams in Figures 10-11, including dashed extrapolations of best fitted trends by HMDs (purple), LMDs (green) and nephelinites-carbonatites (red), together with mineral compositions (Supplementary data D). Reversed modelling trend intersections with olivine-augite-magnetite phase triangles are converted onto ternary plot in Figure 10(g). Thin black lines with boxed ends represent dyke margin-core pairs for samples 519750A to -51 (open squares) and 519768 to-68C (filled squares). Compositions of four ocelli (yellow) were calculated from their phase proportions in Figure 7 and stoichiometric phase formulae.

For the seven major oxides (two of which were combined into total alkalis) that were consistently SEM spot analysed, central clusters were used as nodes to various phase triangles, where the one defined by olivine, augite and magnetite (Fig. C1) is the largest. Visually best fitted trends through both the HMD- and LMD data were extrapolated through these phase-triangles and measured intersections through each of its two limbs (only shown on Fig. C2) were transferred onto a ternary plot in Figure 10(g), for further interpretations discussed in the main text. The same procedure was

repeated for smaller augite-magnetite-biotite phase triangles in Figure C2, from which intersections were transferred on the ternary plot in Figure 10(h).

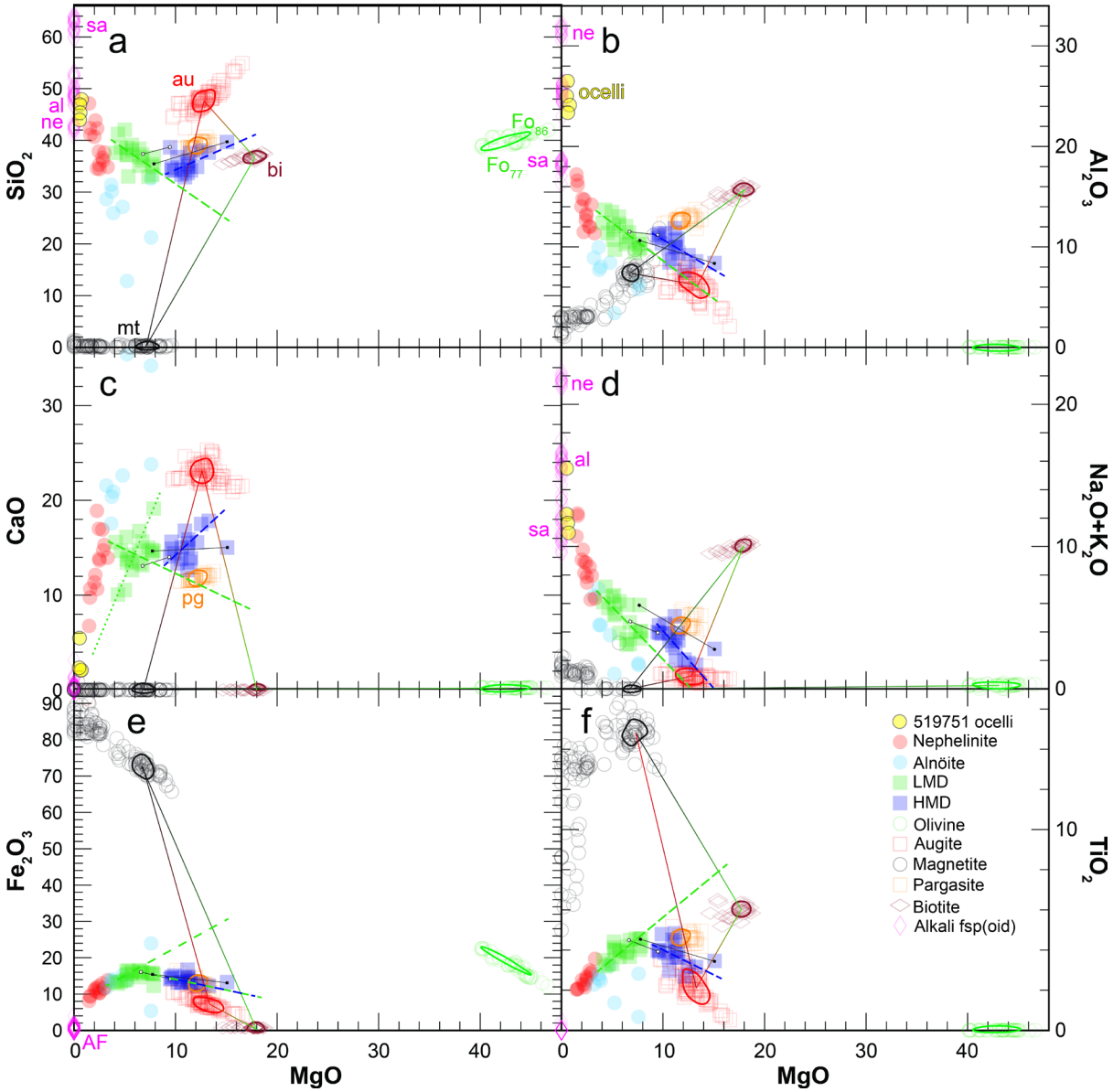

Figure C3: As in Figure C2, but for smaller augite-magnetite-biotite phase triangles and where its margin intersections are transferred onto Figure 10(h). Intersections are just not labelled/quantitated by ratio proportions, as in Figure C2.

Both ternary plots in Figure 10(g-h) roughly exhibit identical areas of intersections between transferred lines for each group of either HMD- of LMD trends, signifying the range of possible assemblages of either olivine, augite and magnetite or augite, magnetite and biotite. Reasons for why results do not cluster even better than this, relate to inaccuracies in regressing data trends, restrictions to only three phases, as well as fractionation/accumulation processes. As examples of the latter, bulk rock compositions may not necessarily conform to well defined liquid lines of descents, or, alternatively, either *in situ* flow segregation of phases or the tapping of crystal mushes from a central magma dyke source were far from perfect. Despite these many potential sources of errors, we find that the model's constraints on likely phase assemblages are significant enough to argue for the fractionation of more magnetite, together with augite and either olivine, biotite, or another mafic phase, from LMD dyke margins (or an equally differentiated central magma chamber source), while HMD dyke cores accumulated much less magnetite, through either of these two processes.

References

JOLLY, R.J.H. & SANDERSON, D.J., 1995. Variations in the form and distribution of dikes in the Mull swarm, Scotland. *Journal of Structural Geology* **17**, 1543-1557.

KLAUSEN, M.B., 2006. Geometry and mode of emplacement of dike swarms around the Birnudalstindur volcano, SE Iceland. *Journal of Volcanology and Geothermal Research* **151**, 340-356.